

## **Double-rowed teeth: design specialization of the *Harpegnathos venator* ants for enhanced tribological stability**

Wei Zhang<sup>a</sup>, Zhigang Wu<sup>a</sup>, Zixin Wang<sup>b</sup>, Zhe Wang<sup>c, d</sup>, Chuchu Li<sup>e</sup>, Hamed Rajabi<sup>f, h, \*</sup>, Jianing Wu<sup>a, \*</sup>

<sup>a</sup> School of Aeronautics and Astronautics, Sun Yat-Sen University, Guangzhou, 510006, People's Republic of China.

<sup>b</sup> School of Engineering and Technology, China University of Geosciences, Beijing, 100083, People's Republic of China.

<sup>c</sup> Beijing Engineering Research Center of Radiographic Techniques and Equipment, Institute of High Energy Physics, Chinese Academy of Sciences, Beijing, 100049, People's Republic of China.

<sup>d</sup> Jinan Laboratory of Applied Nuclear Science, Jinan, 250031, People's Republic of China.

<sup>e</sup> Functional Morphology & Biomechanics, Zoological Institute, Kiel University, Am Botanischen Garten 9, 24118 Kiel, Germany.

<sup>f</sup> Functional Morphology & Biomechanics, Zoological Institute, Kiel University, Am Botanischen Garten 9, 24118 Kiel, Germany

<sup>h</sup> Division of Mechanical Engineering and Design, School of Engineering, London South Bank University, London, UK.

\* Authors to whom correspondence should be addressed.

E-mail addresses: harajabi@hotmail.com (Hamed Rajabi); [wujn27@mail.sysu.edu.cn](mailto:wujn27@mail.sysu.edu.cn) (Jianing Wu).

### **Abstract**

The ant *Harpegnathos venator* can engage in various labors using a pair of elongated mandibles with the ability to rotate about two orthogonal axes. This biaxial rotation enables the ant to gently handle their small, fragile eggs with enhanced contact area and smaller work space. However, how this biaxial rotation influences the ant's predation ability and how the ant responds to this influence remain elusive. We quantitatively investigate the tribological performance of the ant's mandibles during interactions with prey by taking morphology and kinematics into consideration. We find that each ant mandible features unique, double-rows of dorsal and ventral teeth, which are employed to firmly clamp prey over a wide range of sizes by biting their different body parts, demonstrating the ant's predation ability. We hypothesize the mechanism underlying such an ability may rely on the two, non-parallel rows of teeth which potentially eliminate effects of biaxial rotation. To test this hypothesis, we systematically change the distribution and orientation of teeth on bio-inspired robotic mandibles and investigate the mandible tribological performance of different teeth configurations. We find that the friction coefficient varies prominently between the dorsal and ventral teeth resulting from biaxial rotation, with the variations showing an inverse pattern. This explains the observed phenomenon that mandibles equipped with dorsal and ventral

teeth provide the most stable friction coefficient when clamping objects of different sizes using different mandible regions. The specialized distribution of teeth facilitates enhanced tribological stability in capturing prey, and demonstrates an intrinsic link between the form, motion, and function in the insect appendages. Our research sheds lights on the current understanding of the predation behaviors of ants, and can inspire future design of multifunctional robotic grippers.

**Key words:** Ant mandible, mandible morphology, biaxial rotation, prey capture, bioinspiration, biomechanics, tribological stability

## 1 Introduction

Among the many different groups of predaceous insects, diverse forms and behaviors are employed to catch, manipulate, and consume prey (Weseloh and Hare, 2009). Some insects use passive strategies, such as traps as those employed by antlions (Myrmeleontidae) (Allen and Croft, 1985). Others employ active predation strategies; sometimes they contend in fierce fights against struggling prey, which means they must be equipped with effective tools to quickly locate, capture, and incapacitate their food. For example, larval dragonflies and damselflies (Odonata) have prehensile, grasping mouthparts that can be instantly shot out to capture aquatic prey, such as mosquito larvae or dragonfly larvae (Büsse et al., 2021; Resh and Cardé, 2009).

For predatory ants, solitary hunting is the most frequently employed method and the predation strategies and mandible morphologies and kinematics involved are often species specific (Cerdá and Dejean, 2011). Trap-jaw ants, for example, rely on the ultrafast movements of their specialized mandibles to generate extreme forces to strike prey (Gronenberg et al., 1997). *Odontomachus chelifer* has strong mandibles that can be shut together at ultra-fast speeds (on average 39.81 m/s), generating extreme striking forces 371-504 times their body weights to stun prey (Patek et al., 2006; Spagna et al., 2009). The “trap-jaw mechanism” is achieved in diverse ways (Gronenberg, 1996; Booher et al., 2021). Ants of the genus *Acanthognathus* are equipped with mandibles that rotate biaxially to manipulate its mandibles rapidly (Gronenberg et al., 1998a). The mandibles rotate in a ventrolateral direction, which releases opened mandibles that are initially locked by two accessory processes at an average speed of 30°/ms. During this action, the three-pronged tips with fang-like apical teeth penetrate the prey (Gronenberg et al., 1998a).

Another remarkable example is the genus *Harpegnathos*, which is known for its jumping ability, optical sensing, and forceps-like mandibles. These enable the ants to catch cockroaches, crickets, and even spiders up to 10 times their body size (Zhang et al., 2020b; Urbani et al., 1994). The ant *Harpegnathos venator* has a pair of specialized, elongated mandibles (**Fig. 1A,B**) that feature a unique combination of geometries and kinematics: proximal concavities, pointed teeth, and, like *Acanthognathus*, biaxial rotation (Zhang et al., 2020b). Unlike *Acanthognathus*, mandibles of *H. venator* rotate in a dorsolateral direction (Zhang et al., 2020a). Furthermore, the mandibles of *H. venator* close at only 6°/ms on average, much slower than that of the trap-jaw ants, enabling more controlled output of force. These peculiar mandibles can generate forces across five orders of magnitude from 2  $\mu$ N to 200 mN, enabling the ant to engage in a large range of tasks from delicate

jobs like carrying ant eggs to powerful movements like snapping a spider's leg (Zhang et al., 2020b).

Indeed, multifunctional grippers capable of performing versatile tasks pose design and analytic challenges for engineering. To overcome this challenge, many model and robot designs have been developed by mimicking organisms; most of these designs rely on compliance of soft materials, such as soft grippers inspired by a blood-worm (Sui et al., 2020), or an octopus (De Falco et al., 2017). Despite the great progress in soft robotic grippers for universal grasping, multifunctional grippers made of rigid materials are really rare in the existing studies (Liu et al., 2020). Given the advantages on control accuracy, response time and lifespan, developing rigid multifunctional grippers may give rise to reliable solutions for engineering problems. The dexterous mandibles of *H. venator* exhibit significant potentials for rigid multifunctional gripper prototypes (Zhang et al., 2020b). Therefore, fully understanding the mechanism facilitating the ant clamping dexterously may inform the areas of rigid versatile robotic grippers development.

Previous research has partially investigated the multifunctional mechanism behind the ant mandibles. It is validated that the ant *H. venator* employed a biaxial rotation pattern to manipulate smooth concavities on the proximal parts of the mandible to interact with its small, fragile eggs (**Fig. 1B**) (Zhang et al., 2020b). Compared to uniaxial rotation, biaxial rotation combined with specific concavities can grip eggs with a greater contact area and at a smaller workspace (Zhang et al., 2020a). Although how the ant performs gentle gripping has been uncovered, little is known about the mechanism underlying its predation ability using biaxially-rotated mandibles. Regardless of the benefits of the biaxial rotation to brood care, it may negatively affect the ant's predation ability, due to the induced alteration of mandible postures (McIntosh et al., 2006). Generally, the ant uses its mandibles to firmly clasp prey with a powerful friction force generated by penetrating mandible teeth into their bodies. The friction force is closely related to geometries and orientations of mandible teeth. Although the geometry of a given mandible tooth is invariable normally, its orientation will change if the mandible rotates biaxially, and consequently influence the tribological performance (McIntosh et al., 2006). An open question that cannot be fully answered with the existing data: how do the ant mandibles combine requirements for two functions that demand different tools. The morphology and kinematics of the mandibles, in particular the exact geometry of the teeth and the biaxial rotation pattern, have only been partially investigated (Zhang et al., 2020a). Furthermore, the exact influence of the specific mandible morphology and the double-rowed teeth on the tribological performance of the mandibles has not been sufficiently studied.

In this study we mainly focus on the mandible tribological performance in the predation behaviors of *H. venator* ants by taking biaxial rotation into consideration. Scanning electron microscopic imaging and micro-CT imaging are utilized to visualize the morphology of the mandible teeth and the joint between the mandible and head. Experimental observations of the ant's predation behavior are conducted to quantify the size range of captured prey. Considering the morphology and the biaxial rotation, the tribological performance of the mandibles during interaction with prey items, described by normal and friction forces as well as friction coefficient,

are predicted by theoretical modelling and verified by five paradigms of robotic mandibles. The biological and engineering implications of these findings are discussed.

## **2 Materials and methods**

### **2.1 Sample collection**

About 100 ants of the species *H. venator* were collected from Guangzhou, Guangdong, China (23°7' N, 113°15' E) and identified according to a previous literature (Donisthorpe, 1937). These ants were kept in artificial nests at a constant temperature of 25°C and humidity of 60%. All ant specimens were fed with living cockroaches (species *Blatta lateralis*) every three days. Only worker ants were used in the experiments.

### **2.2 Scanning electron microscopy**

Six head samples from ant workers were cut off, submerged in 2.5% glutaraldehyde for 3 h at 25°C, washed with 0.1 mol/L phosphate buffer three times, and dehydrated in a graded ethanol series (75%, 80%, 85%, 90%, 95% and 100%) for 12 h before freeze drying. These samples were sputter-coated with ~9 nm gold palladium and then imaged using a scanning electron microscope (FEI Quanta 200, Czech Republic) in a high-vacuum condition at 15 kV.

### **2.3 Micro-CT imaging**

To determine the morphology of the mandibular articulation, two head samples were first cut off and then the right mandibles were removed by a pair of surgery scissors (Jinggong, China) to expose the mandibular articulations. The prepared specimens were scanned using a spectral Micro-CT scanner (Institute of High Energy Physics, Chinese Academy of Science, Beijing, China) at a voltage of 50 kV, a current of 160  $\mu$ A, an exposure time of 270 ms, spatial resolution of 8.3  $\mu$ m, and a rotation angle of 0.18°. The raw data was imported into the software Mimics (Version: 17.0, Materialise NV, Belgium) to create the 3D reconstructions. The holes and irregular surfaces were carefully removed to improve the quality of the 3D reconstructions.

### **2.4 Observation of predation behaviors**

Prior to predation behavior experiments, the ants were starved for 12 h. Then one ant and one cockroach (*Blatta lateralis*) were placed in a petri dish (8.6 mm in diameter and 1.3 mm in depth) and the preying process was recorded by a camera (Canon, EOS 6D, Japan) with a macro lens (Canon, EF100mmf/2.8LISUSM, Japan) from the dorsal view. Forty ant workers were recorded in this manner.

### **2.5 Measurements of normal and friction forces in bio-inspired robotic mandibles**

To analyze respective effects of the dorsal and ventral teeth on tribological performance, five types of artificial mandibles were modeled in the software Solidworks (Dassault Systèmes, France), scaled up by 100 times the normal size and fabricated with photosensitive resin material (RS-F2-GPWH-04, Formlabs, USA) using a 3D printer (Form 2, Formlabs, USA) (**Fig. 1C**). The photosensitive resin featured high rigidity and strength, similar to the property of the strongly sclerotized cuticle that makes up the ant mandibles (Gronenberg et al., 1998b). The morphological configurations of these mandibles included one or two rows of teeth, mimicking the dorsal (D)

and/or ventral (V) teeth of the *H. venator* mandibles as described in **Table 1**. Although the number of teeth of these artificial mandibles was different, the volume of a single tooth was approximately 0.28% of the artificial mandible and consequently the amount of material used to make these artificial mandibles was unified. To account for mandible posture variation caused by the biaxial rotation, versions of each type of mandible rotated at angles of 0°, 10°, 20°, 30°, and 40° along the long axis were constructed in Solidworks and fabricated by 3D printing technique. Then the tribological performance was quantified by measuring normal and friction forces of these robotic mandibles. To measure the normal force, we customized a fixture to connect the artificial mandibles to a force sensor (GSO-30, Transducer Techniques, USA) that was fixed to a stepping motor (HST01, China) in the vertical direction. Then we controlled the stepping motor to actuate the artificial mandibles so that the teeth were gradually inserted into the gel substrate at a velocity of 0.5 mm/s vertically until the mandibles surface contacted to the gel substrate (Das and Ghatak, 2011). The normal forces during this process were recorded and displayed by the software SENSIT (FUTEK, USA) (**Fig. 1D**). To examine the friction force, the artificial mandibles were first mounted to the force sensor (GSO-30, Transducer Techniques, USA) by a customized fixture in the horizontal direction. Subsequently, we manually pressed the mandibles on the surface of the gel substrate in a tank until the teeth were completely inserted into the substrate. Then the tank with gel substrate were pulled by a stepping motor (HST01, China) at a velocity of 0.5 mm/s horizontally for 10 s (**Fig. 1E**). The friction force was then measured by the force sensor and collected by the software SENSIT (FUTEK, USA). The force sensor was calibrated before and after each trial to eliminate the effects of gravity. Each robotic mandible was examined three times to minimize the potential influences of randomness and uncertainties in the experiment.

**Table 1 Morphology of five types of artificial mandibles.**

Type	Surface morphology
DT	Only one row of dorsal teeth
VT	Only one row of ventral teeth
DDT	Both rows of dorsal teeth
VVT	Both rows of ventral teeth
DVT	Both rows of dorsal and ventral teeth

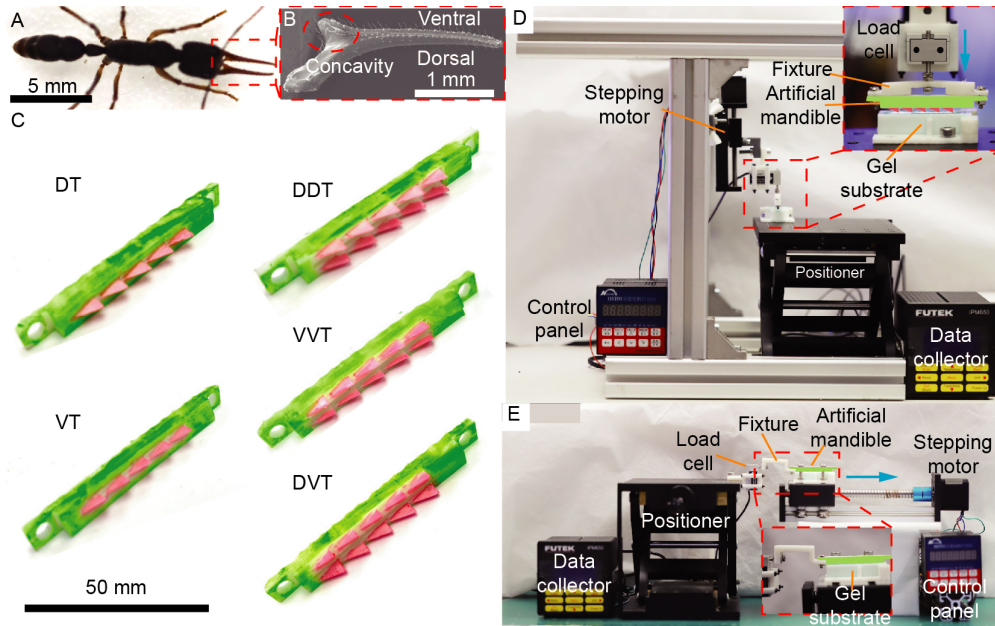


**Fig. 1** The ant *H. venator* and its mandibles, as well as schematics of five artificial mandibles with different tooth configurations and setups for testing the normal and friction forces of these mandibles. (A) The ant *H. venator*. (B) The ant's mandible. (C) Five types of artificial mandibles with various surface configurations. Experimental setups for measuring (D) normal force and (E) friction force generated by artificial mandibles painted green.

### 3 Results

#### 3.1 Morphology of the mandible and head-mandible joint

The ant mandible has a length of  $3.69 \pm 0.57$  mm ( $n=6$ ) and can be subdivided into two parts according to their morphologies (**Fig. 2A**). Part I, closer to the ant head, has a length of  $l_1 = 1.03 \pm 0.17$  mm ( $n=6$ ) and makes an angle of  $\phi_0 = 60.44 \pm 2.36^\circ$  ( $n=6$ ) to the ant head when the mandibles are closed. No sharp teeth and bristles are found on part I (**Fig. 2A**). Part II has a length of  $l_2 = 2.83 \pm 0.16$  mm ( $n=6$ ) and is perpendicular to the ant head when the mandibles are closed. Part II possess two rows of sharp teeth, with a row of bristles in between (**Fig. 2B**). Notably, the dorsal and ventral teeth are not parallel to each other (**Fig. 2B**). Specifically, the dorsal teeth are tilted and make an angle of  $\gamma = 33.17 \pm 5.58^\circ$  ( $n=6$ ) to the mandible. In contrast, the ventral teeth stand almost perpendicular to the mandible surface (**Fig. 2B**). The dorsal and ventral teeth are triangular pyramid-shaped, with  $a = 26.60 \pm 7.65$   $\mu\text{m}$ ,  $b = 35.79 \pm 4.57$   $\mu\text{m}$ ,  $\psi = 67.91 \pm 12.71^\circ$  and  $h_N = 74.46 \pm 19.29$   $\mu\text{m}$  ( $n=6$ ) (**Fig. 2B**).

**Fig. 2C** and **2D** shows the joint between the mandible and the head. The subpart on the mandible is termed 'spindle' (**Fig. 2C**) and the joint part in the head is a 'pivot' where a sector bulge determines the motion trail of the mandibles (**Fig. 2D, 2E**). Together, these comprise a cylindrical hinge. Micro-CT imaging of the joint (**Fig. 2F**) shows that the pivot in *H. venator* is not in a dorsoventral direction like in other ant species (Richter et al., 2019), but instead is at an angle of

$\theta = 44.17 \pm 4.24^\circ$  to the horizontal plane ( $n=2$ ). The rotation about the inclined axis can be decomposed into two concurrent rotations about two orthogonal axes, thus changing the mandible posture (McIntosh et al., 2006).

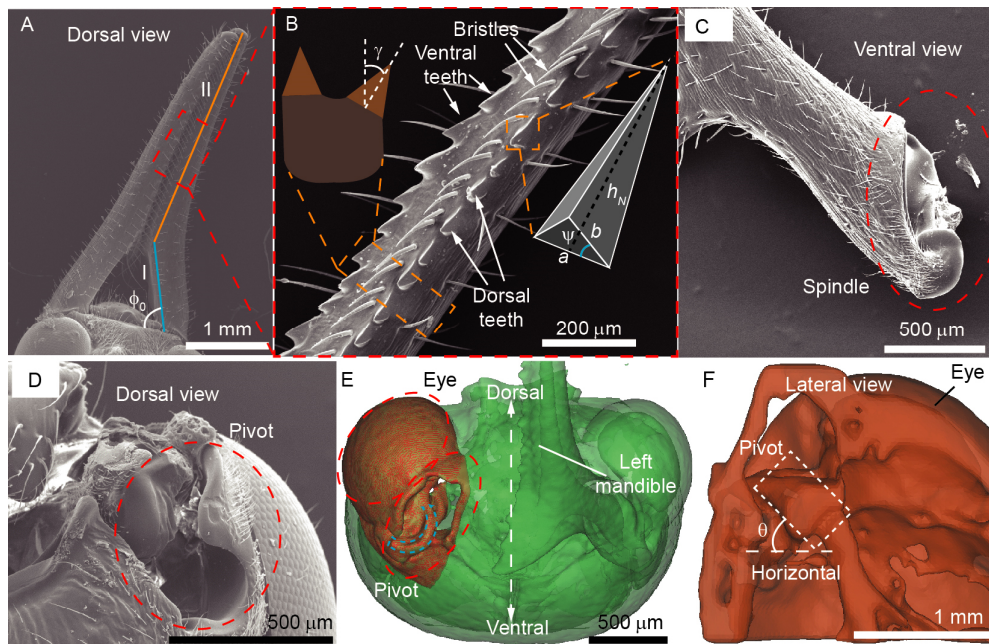


**Fig. 2 Morphology of the ant mandibles and mandibular joints.** (A) The ant mandible (dorsal view) is divided into parts I and II.  $\phi_0$ , the angle between part I and the head. (B) Middle section of the right mandible and the geometry of the teeth.  $a$  and  $b$ , the lengths of two sides in the lateral triangular face of a tooth;  $\psi$ , the angle in between the two sides;  $h_N$ , the height of the bottom triangular face. (C-D) The connection joint comprised of a spindle (ventral view) (C) and a pivot (dorsal view) (D). (E-F) Micro-CT images of the ant head (frontal view) (E) and the pivot (lateral view) (F).  $\theta$ , the angle of the pivot to the horizontal plane.

### 3.2 Predation behaviors

We record successful hunting of 40 ant workers. Each preying event has four distinguishable stages: detection, positioning, clamping, and stinging (**Fig. 3A**). Once the ant senses the prey visually, it orients its body towards the prey, opens its mandibles and latches onto the prey tightly, followed by stinging to paralyze the prey (**Fig. 3A**). Each ant could capture cockroaches that have a broad range of body lengths, from 5 mm to 15 mm (**Fig. 3B**, **Supplementary Video S1**). In addition, the ants express high flexibility in clamping on different prey body parts; they frequently clamp on legs, head, thorax, and abdomen, each of which differs considerably in size (**Fig. 3B**). Accordingly, we introduce a featured dimension  $d$  defined by the size of each body part along the clamping direction of the ant mandibles, such as leg diameter, thorax thickness, head width, and apodeme width. As shown in **Fig. 3C**, an ant could open its mandibles by up to  $40^\circ$  in the horizontal plane to grasp objects from 0.1 mm to 3.1 mm, a 31-fold difference. Interestingly, when clamping on body parts with the same featured dimension, the rotation angle of the mandibles is not constant.

**Fig. 3C** shows that the rotation angle for clamping 1.25-mm body parts varies from  $20^\circ$  to  $34^\circ$ . Moreover, with a constant rotation angle, the mandibles can grip body parts with different featured dimensions. For example, when the mandibles rotate  $30^\circ$  in the horizontal plane, the featured dimension of the body parts held by the ant ranges from 1.08 mm to 3.08 mm (**Fig. 3C**). That is likely because the ant can employ different regions of its mandibles to contact objects.

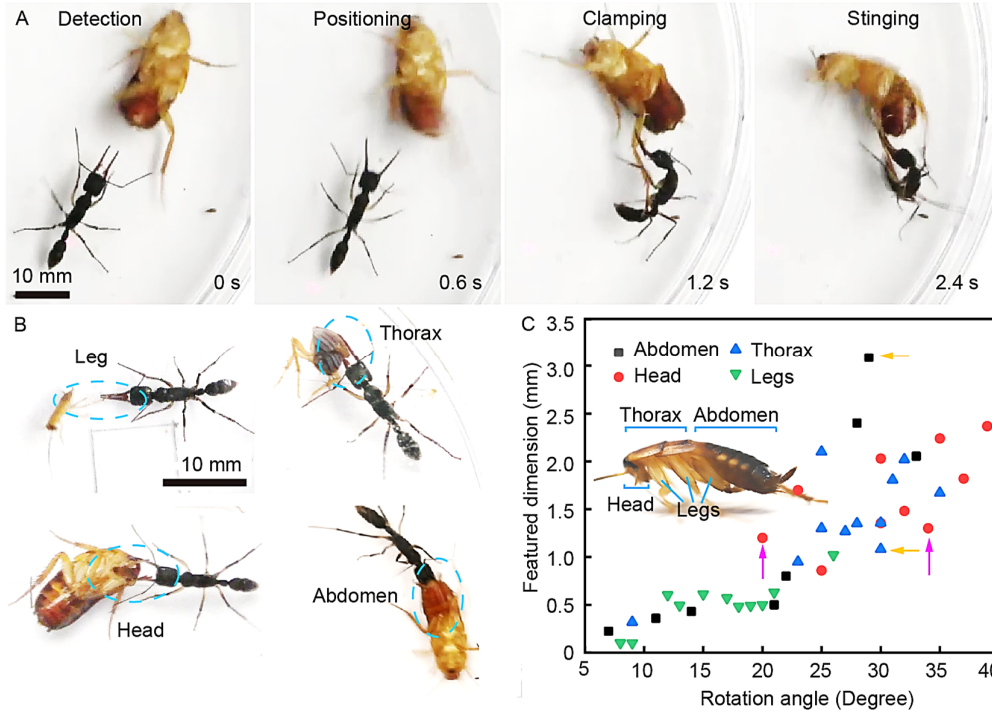


**Fig. 3 Predation behavior of *H. venator*.** (A) Four stages of the ant preying on a cockroach (*Blattella lateralis*). (B) The ants can capture prey of various sizes by clamping different body parts, including the leg, thorax, head, and abdomen. (C) The measurements of the mandible rotation angle in the horizontal plane and the corresponding featured dimension of the clamped body parts of prey. Orange arrows denote that the ant clamped body parts of different  $d$  with the same rotation angle. Pink arrows represent that the ant grasped body parts of the same  $d$  with different rotation angles.

### 3.3 Theoretical modelling

To quantitatively reveal how the featured dimension of the prey and the employed region of the ant mandibles impacted tribological performance, we propose a theoretical modelling in terms of kinematics and biomechanics. We use our results to predict the dynamic positions and postures of the mandibles, and analyze the contact forces between the mandible and the prey (**Fig. 4**).

A global coordinate frame  $G$  and a local coordinate frame  $L$  are defined (**Fig. 4A, B**). In the  $G$ -frame, the origin  $O$  is placed at the connection joint,  $X^G$  is aligned with the long axis of the ant head,  $Y^G$  is in the horizontal plane and vertical to  $X^G$ , and  $Z^G$  is determined by the right-handed system (**Fig. 4A**). The  $L$ -frame is fixed to the left mandible and consistent with the  $G$ -frame when the mandibles are closed (**Fig. 4B**). The position of the inclined axis  $e$  in the  $G$ -frame could then

be derived as  $e = (\sin \theta, 0, \cos \theta)$ , where  $\theta$  is  $45^\circ$  (Zhang et al., 2020a). When the ant mandible rotated  $\tau$  around  $e$ , the rotation of the mandible can be decomposed into two orthogonal components: one about  $X^G$ -axis and another about  $Z^G$ -axis (**Fig. 4A**). Given  $\theta = 45^\circ$ , the rotation angles of the two components are equal, and can be calculated by

$$\alpha = \tau \sin \theta \quad (1)$$

Considering the mandible morphology, we model each mandible as two rods: rod I with a length of  $l_1$  made an angle of  $\phi_0$  with the ant head, and rod II with a length of  $l_2$  perpendicular to  $X^G$ -axis (**Fig. 4B**). When the mandibles are closed, a randomly selected point  $Q$  on rod II is initially situated at point  $Q_0 = (x_0, y_0, z_0)$  in both the  $L$ -frame and  $G$ -frame (**Fig. 4B**). As shown in **Fig. 4B**, as the ant mandible rotates  $\tau$  around the inclined axis  $e$ , the new position of the same point, i.e.  $Q_1^G = (x_1, y_1, z_1)$ , in the  $G$ -frame can be expressed as

$$Q_1^G = R_\tau Q_0 \quad (2)$$

where the transformation matrix  $R_\tau$  is  $R_\tau = \cos \tau I + (1 - \cos \tau) e \times e^T - \sin \tau (e \times)$  and  $I$  is a  $3 \times 3$  unity matrix (Giulietti and Tortora, 2007). Due to the symmetry of mandibles, the mandibular distance  $d_Q$  at the selected point  $Q$  can be calculated by

$$d_Q = 2|y_1 - y_0| \quad (3)$$

If the region is used for gripping, the mandibular distance  $d_Q$  should be equal to the featured dimension  $d$  of the clamped object. Thus, the angle  $\tau$  that the mandible should rotate can be calculated by solving equations (2) and (3) with a known  $Q$  and  $d$ . Then the rotation angle  $\alpha$  about  $X^G$ -axis can be obtained correspondingly (equation (1)). Since this biaxial rotation alters mandible's posture, the angle of the dorsal teeth to the horizontal plane changes from  $\gamma$  to  $\gamma - \alpha$  and the ventral teeth from 0 to  $\alpha$  (**Fig. 4C**).

**Fig. 4D** schematically shows the penetration of a tooth into an object (here prey's body) under a normal force  $P$ , generating a friction force  $F$  because of plowing effect (Bhushan and Nosonovsky, 2004; Brito et al., 2017). Hence, both the normal and the friction forces can be determined by the projection area of the tooth and the yield strength of the object's material (Bhushan and Nosonovsky, 2004). As shown in **Fig. 4D**, the projection area of the tooth in the  $X^G O Z^G$  plane is

$$S_N = ch_N / 2 \quad (4)$$

where  $h_N$  can be measured (**Fig. 2B**) and  $c$  can be determined by

$$c = \frac{a \sin \beta (b \cos(\psi - \beta) - a \cos \beta)}{b \sin(\psi - \beta) + a \sin \beta} + a \cos \beta \quad (5)$$

Here  $\beta$  indicates the angle between the tooth and the horizontal plane (**Fig. 4D**),

$$\beta = \begin{cases} \gamma - \alpha, & \text{Dorsal teeth} \\ \alpha, & \text{Ventral teeth} \end{cases} \quad (6)$$

By defining the compressive yield strength of the material as  $\sigma_N$ , the normal force  $P$  could be calculated by (Bhushan and Nosonovsky, 2004)

$$P = \sigma_N S_N = \sigma_N ch_N/2 \quad (7)$$

As illustrated in **Fig. 4D**, the projection area  $S_F$  of the tooth onto  $Y^G OZ^G$  plane is calculated as follows

$$S_F = ch_f/2 = cb \sin(\psi - \beta)/2 \quad (8)$$

The friction force  $F$  is the product of the shear strength  $\sigma_F$  of the object's material and the projection area  $S_F$  along the force direction, expressed by (Bhushan and Nosonovsky, 2004)

$$F = \sigma_F S_F \quad (9)$$

According to equations (6), (8) and (9), the friction force is proportional to  $S_F$  and varies with respect to the rotation angle  $\alpha$ .

The friction coefficient  $f$ , defined as the ratio of friction force  $F$  to normal force  $P$ , can be written as

$$f = F/P = b \sin(\psi - \beta) \sigma_F / h_N \sigma_N \quad (10)$$

Assuming that the material of the object is isotropic, i.e.  $\sigma_N = \sigma_F$ , equation (10) can be written as

$$f = F/P = b \sin(\psi - \beta) / h_N \quad (11)$$

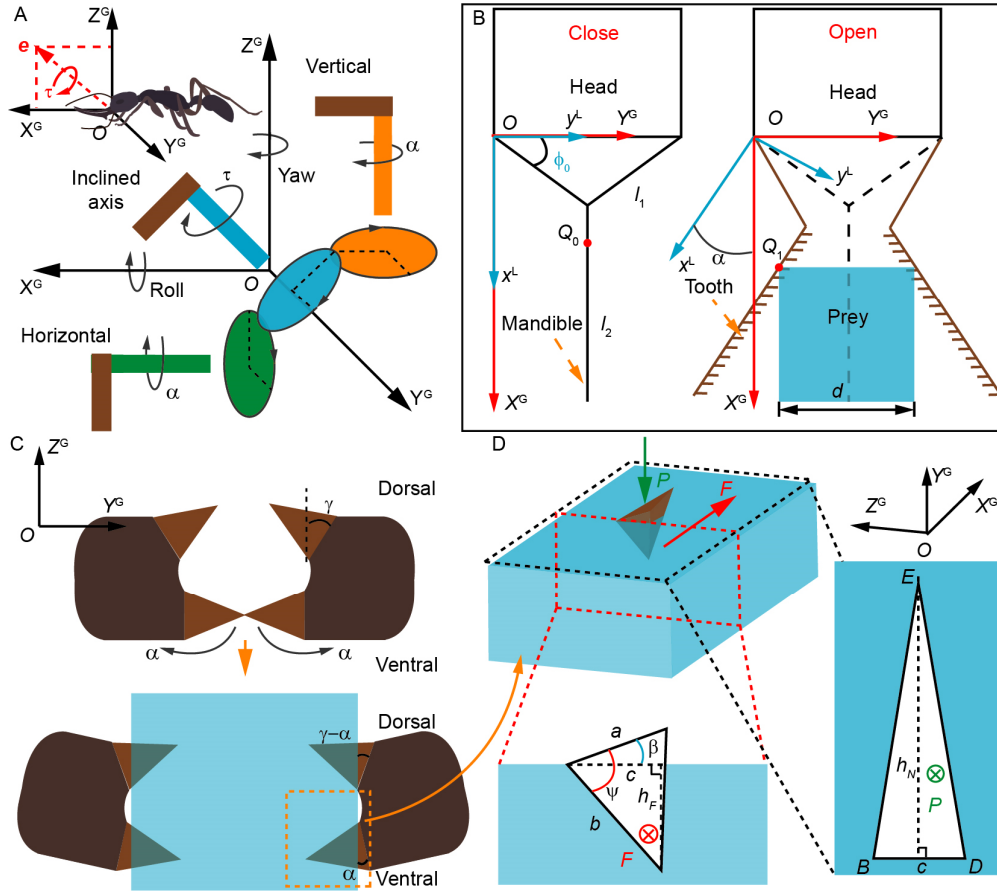


**Fig. 4 Schematic of the theoretical modelling.** (A) The biaxial rotation means that the ant mandible rotates about the inclined axis  $e$  (blue shape), which can be decomposed into two components, including yawing about  $Z^G$ -axis (orange shape) to open/close in  $X^G O Y^G$  plane and rolling about  $X^G$ -axis (green shape), changing the mandible posture in  $Y^G O Z^G$  plane. The rotation angle about  $Z^G$ -axis or  $X^G$ -axis is  $\alpha$ , while that about  $e$  is  $\tau$ . Brown shape denotes the ant mandible. (B) Modeling the opening of mandibles by  $\alpha$  degree to clamp an object of featured dimension  $d$  at the new position of point  $Q$ . The left inset shows the fully closed mandibles and the right illustrates the mandibles clamping the prey. (C) Schematic drawing of the frontal view of dorsal and ventral teeth when inserted into an object. The upper inset presents the initially closed mandibles and the lower shows the teeth, whose postures are altered by biaxial rotation when inserted into the object. (D) Illustration of a tooth inserted into an object. The part of the tooth penetrating the object is projected onto plane  $Y^G O Z^G$  and plane  $X^G O Z^G$ . The former projection has a side length of  $c$  and a height of  $h_F$ . The latter has a side length of  $c$  and a height of  $h_N$ . The angle between  $a$  and  $c$  is defined as  $\beta$ . Here  $P$  and  $F$  denote the normal and friction forces, respectively.

### 3.4 Tribological performance

We 3D print five types of artificial mandibles with different morphologies (DT, VT, DDT, VVT and DVT, as defined in **Table 1**) and compare their tribological performance (**Fig. 1C**). We use the 3D printed mandibles to estimate the normal and friction forces of dorsal and ventral teeth with

various rotation angles  $\alpha$  about  $X^G$ -axis. Using the experimentally measured normal and frictional forces of the five types of 3D printed mandibles (in  $\alpha = 0^\circ$ ), the compressive and shear moduli of the gel substrate are estimated to be  $\sigma_N = 24.67 \pm 7.68$  kPa and  $\sigma_F = 22.63 \pm 0.65$  kPa, which fall within the modulus range of the gel material previously reported (Ghatak and Das, 2007). Considering the small difference between  $\sigma_N$  and  $\sigma_F$  (8% only), the substrate is regarded as an isotropic material with the modulus of  $\sigma_s = 23.65$  kPa, equal to the average value of  $\sigma_N$  and  $\sigma_F$ . Hereby, the normal force  $P$ , the friction force  $F$ , and the friction coefficient  $f$  of the five types of artificial mandibles are theoretically calculated by parametrically sweeping the rotation angle  $\alpha$  ( $0^\circ \sim 45^\circ$ ), covering the full range of mandible rotation of the ant from  $0^\circ$  to  $40^\circ$  (**Fig. 3C**).

We plot the data of theoretical modelling, including normal force  $F$ , friction force  $P$ , and friction coefficient  $f$  for the five types of the robotic mandibles (**Fig. 5A-C**). The corresponding experimental measurements are also presented to quantify the accuracy of the theoretical modelling. Among the five types of the robotic mandibles, the respective greatest differences between the theoretical and the mean experimental values of friction force, normal force, and friction coefficient are 8.68%, 9.93% and 17.12%. The good agreement between the two sets of data suggests that our theoretical modelling can predict the tribological performance accurately.

While hunting, the ant requires sufficient normal force to drive mandible teeth to penetrate the prey exoskeleton and generate friction force. Therefore, the magnitude of the normal force played a key role in tribological performance. The respective normal forces that enable five types of robotic mandibles to insert gel substrate are presented in **Fig. 5A**. The normal force does not keep constant as rotation angle increases, which results from the change in tooth orientation. Clearly, the normal force for the mandibles with two rows of teeth to insert into the substrate are about twice that of mandibles with only one row of teeth (**Fig. 5A, Table 2**). However, the difference in the mean values of normal force between DT and VT (1.54%) or between DDT, VVT, and DVT (smaller than 2%) is ignorable, meaning that the normal force largely depends on the number of rows of teeth.

As seen in **Fig. 5B**, the friction forces of the five types of robotic mandibles are about one third of their corresponding normal force. Additionally, the friction forces for DT and VT are approximately half of those for DDT and VVT (**Fig. 5B, Table 2**). The friction forces of those robotic mandibles with double rows of teeth show completely different variations with increasing rotation angle, namely ascending for DDT, declining for VVT, nearly constant for DVT. This can be verified by the magnitudes of standard deviations of friction force, as shown in **Table 2**. The standard deviations for DDT and VVT are almost 13 times that for DVT, demonstrating the friction force for DVT does not noticeably change due to the change of the rotation angle (**Fig. 5B, Table 2**). Interestingly, the discrepancy in mean friction force between these three types of mandibles is less than 6%, which means the two, non-parallel rows of teeth reduce the variation in friction force without decreasing its average magnitude.

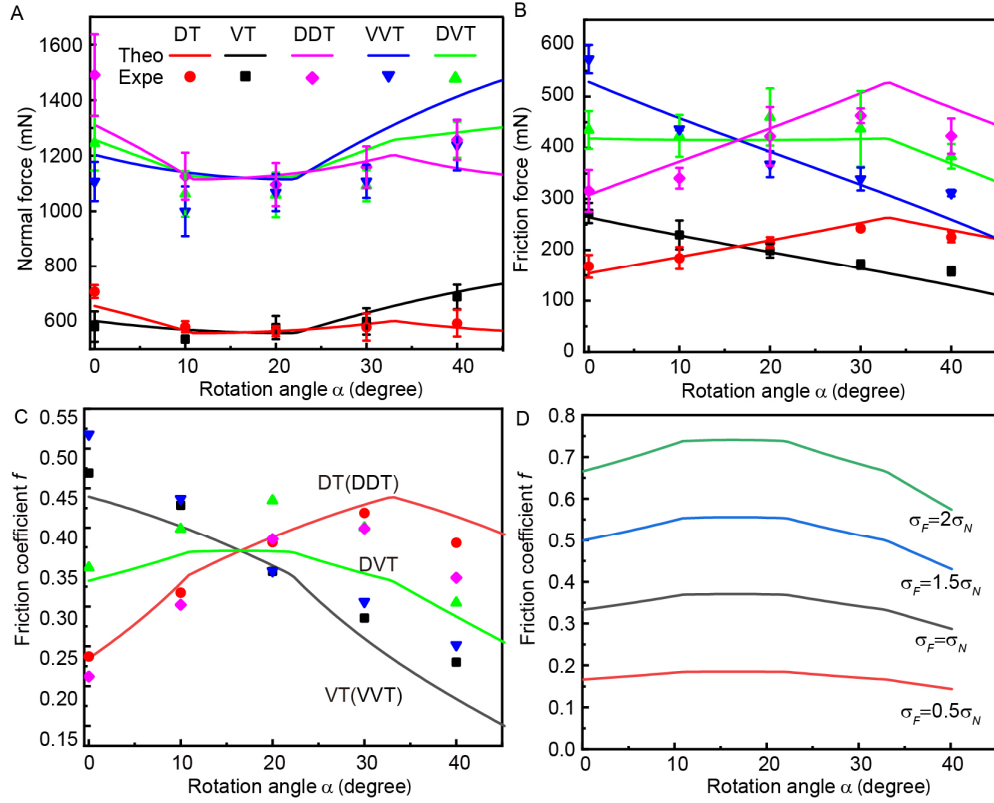


**Fig. 5 Comparison of tribological performance of the mandible models based on the experimental measurements and theoretical modeling.** (A, B) The normal force (A) and friction force  $P$  (B) of five types of bio-inspired robotic mandibles. (C) The friction coefficient  $f$  of the mandibles in different rotation angles  $\alpha$ . Scattered points show average values of the measured  $P$  and  $F$  forces, and lines represent theoretical results. (D) Friction coefficient  $f$  against rotation angle  $\alpha$  for a range of material properties. The brown regions in (A-D) denote the range of the rotation of the real ant mandible.

**Table 2 The mean values and standard deviations of  $F$ ,  $P$ , and  $f$  for the five types of mandibles.**

	Mean value of $P$ (mN)	Standard deviation of $P$ (mN)	Mean value of $F$ (mN)	Standard deviation of $F$ (mN)	Mean value of $f$	Standard deviation of $f$
DT	626.22	40.15	224.70	35.81	0.37	0.06
VT	616.56	26.79	211.76	38.28	0.34	0.07
DDT	1252.43	80.30	449.40	71.62	0.37	0.06
VVT	1233.12	53.57	423.51	76.56	0.34	0.07
DVT	1242.78	56.41	436.45	5.90	0.35	0.02

The relationship between  $f$  and  $\alpha$  for five different mandibles under the condition of  $\sigma_N = \sigma_F$  is shown in **Fig. 5C**. The theoretical  $f$  values of DDT and VVT coincide with those of DT and VT due to the linear relationship between the normal and friction forces and the projection area according to equations (7) and (9) (**Fig. 5C**). As seen in **Fig. 5C**, the degree of change in theoretical  $f$  for DVT is less than for DDT or VVT, consistent with the result that the standard deviation of  $f$  for DVT is the smallest among them (**Table 2**). The mean values of  $f$  between these three types of

mandibles, however, show tiny difference (8% only). This indicates that, compared to two rows of identical teeth, two rows of non-parallel teeth minimize the variation in  $f$  induced by biaxial rotation without compromising the average magnitude, which may be a novel strategy that can empower the ant to adaptively capture prey over a large range of sizes.

We also quantify the influence of the material properties of substrate on  $f$  by setting the ratio of  $\sigma_F$  to  $\sigma_N$  ranging from 0.5 to 2. **Fig. 5D** shows that the  $f$  increases with respect to increasing ratio of  $\sigma_F$  to  $\sigma_N$ . When the ratio increases from 1 to 2, the magnitudes of  $f$  has also doubled and reached up to 0.75. In contrast, when the ratio lowers to 0.5, the  $f$  is smaller than 0.2. Notably, the degree of variation in the magnitude of  $f$  with respect to the rotation angle  $\alpha$  becomes less as the ratio increases (**Fig. 5D**).

### 3.5 Tribological stability

As described in Section 3.2, the ant is observed to clamp objects of a constant  $d$  with different rotation angles in the horizontal plane, and to clasp objects of various  $d$  with the same rotation angle. This is because the mandible region used to contact the object directly can be variable. Hence, the rotation angle about  $Z^G$ -axis is determined by the employed mandible region  $x$  as well as the featured dimension  $d$  of the object. Because of biaxial rotation, the change in rotation angle about  $Z^G$ -axis would alter that about  $X^G$ -axis which is closely relevant to friction coefficient (**Fig. 4A** and **Fig. 5C**). Prior to evaluating the effects of biaxial rotation on friction coefficient through the two parameters, the mandible region  $x$  and the featured dimension  $d$  are parametrically swept to elucidate the rotation angle  $\tau$ . According to the fact that the maximal  $\alpha$  the ant mandible can rotate in horizontal plane is  $40^\circ$ , the upper limit of  $\tau$  is assigned to be  $56^\circ$  (equation (1)). As seen in **Fig. 6A**, the rotation angle  $\tau$  decreases with  $x$  but increases with  $d$ . Notably, at the mandible region of  $x=2.50$  mm, the ant can clasp objects of  $d$  over a range from 0.10 to 3.50 mm by rotating the mandibles at increasing angles biaxially (**Fig. 6A**). In addition, given a 1-mm object, the ant can utilize various mandible regions to clasp it (**Fig. 6A**).

We plot the friction coefficient  $f$  for the five developed mandible models in **Fig. 6B~D**, respectively. Our results suggest that  $f$  for DDT, which is the same for DT, increases from 0.24 to 0.43 for prey of  $d$  ranging from 0.10 mm to 3.50 mm (**Fig. 6B**). The most visible variations in the friction coefficient  $f$  are found in the following two cases: (1) using the same mandible region  $x$  to clamp prey of different  $d$  (as white, dashed line shows), and (2) applying different mandible regions to clamp prey of the same  $d$  (as black, dashed line shows). As for the first case, when the ant uses the mandible region of  $x=2.50$  mm to clamping objects of  $d$  varying from 0.10 to 3.50 mm,  $f$  raises from 0.25 to 0.43 (difference=0.18) (**Fig. 6B**). In the second case, given a 1-mm object,  $f$  for using the region of  $x=1$  mm to clamp it is 0.41; at  $x=3.65$  mm,  $f$  drops to 0.30 (difference=0.11) (**Fig. 6B**).

Similar variation of  $f$  occurs when using VVT or VT to clamp objects, and the values range between 0.18 and 0.44 (**Fig. 6C**). Prominent variations in  $f$  are also found in the two types of robotic mandibles. On one hand, as  $d$  of objects clamped by mandible region of  $x=2.50$  mm ascends from 0.10 to 3.50 mm,  $f$  correspondingly descends from 0.44 to 0.22 (difference=0.22) (**Fig. 6C**). On the

other hand, given a 1-mm object, when the employed regions alter from  $x=1$  mm to  $x=3.65$  mm,  $f$  increases from 0.31 to 0.41 (difference=0.10) accordingly.

Unlike the above types of robotic mandibles, when DVT is used to clamp objects,  $f$  shows smaller variations (**Fig. 6D**). Specifically, for the mandible region of  $x=2.50$  mm,  $f$  for gripping objects of  $d$  from 0.1 mm to 3.50 mm ranges between 0.33 and 0.37 (difference=0.04). Moreover, to clamp a 1-mm object,  $f$  for the mandible regions changing from  $x=1$  mm to  $x=3.65$  mm is between 0.36 and 0.37 (difference=0.01).

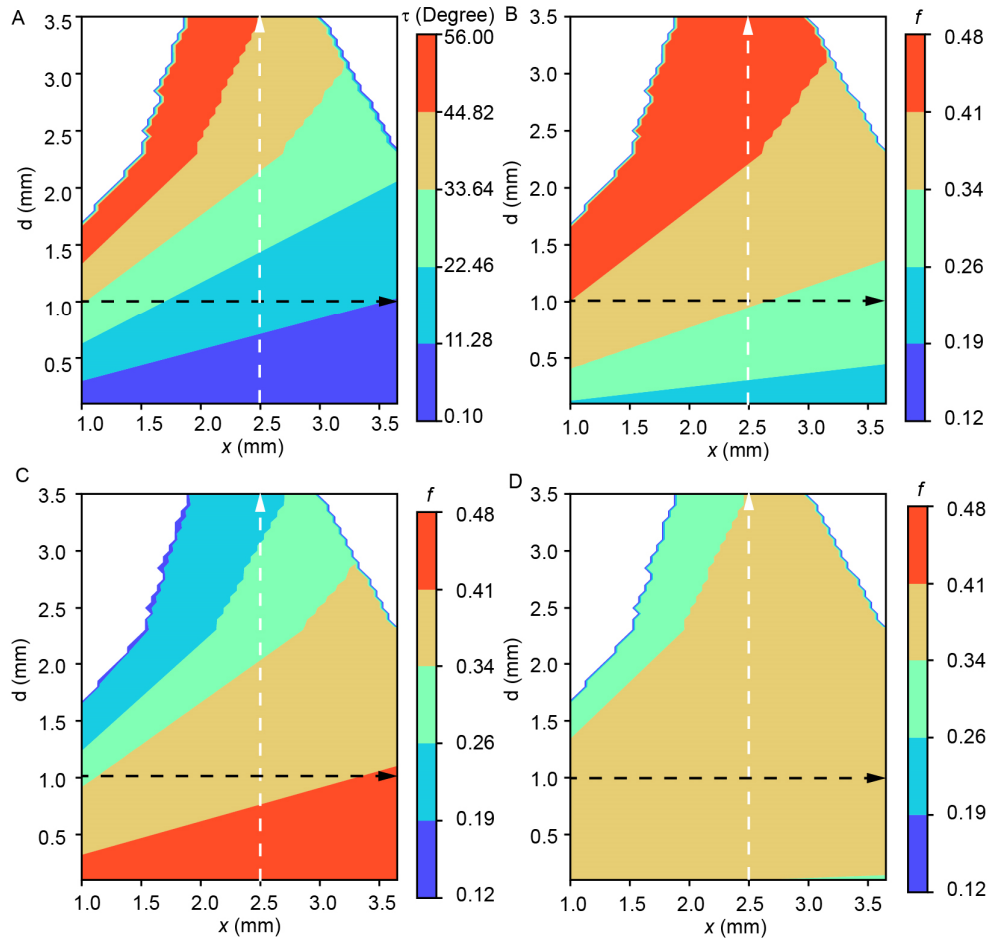


**Fig. 6 Tribological performance of the five developed mandibles when different mandible regions  $x$  are used to clamp objects with various featured dimension  $d$ .** (A) Contour plot of rotation angle  $\tau$ . (B) Contour plots of friction coefficient  $f$  for DDT and DT (B), VVT and VT (C), and DVT (D). Legends denote the range of rotation angle  $\tau$  (A) and friction coefficient  $f$  (B~D). Black, dashed line with an arrow represents the case that an ant clasps a 1-mm object using mandible regions  $x$  varying from 1 to 3.65 mm. White, dashed line with an arrow represents the case that an ant employs the region  $x=2.50$  mm to clasp objects of featured dimension  $d$  varying from 0.10 to 3.50 mm.

## 4 Discussion

The ant *H. venator* is one of only two species known to rotate its mandibles biaxially. Here we

provide the first morphological evidence of biaxial rotation in the ant's mandibles. The ant rotates its mandibles around a pivot that is at an angle of  $\theta = 44.17 \pm 4.24^\circ$  (**Fig. 2F**) to the horizontal plane to perform biaxial rotation, changing the mandibles' positions and postures simultaneously. This observation is in agreement with our previous study, in which we hypothesize that the inclined angle of the rotating pivot should be approximately  $45^\circ$  (Zhang et al., 2020a). Additionally, rotating around an inclined pivot is similar to the way dragonflies flap their wings for hovering with enhanced efficiency (Park and Choi, 2012).

We previously conducted a comparison analysis between the biaxial rotation (real case) and the uniaxial rotation (hypothetical case) in the mandibles of *Harpegnathos venator* and did find that the kinematic pattern plays a key role in mandible performance (Zhang et al., 2020a). The unusual biaxial rotation combined with the specific mandible concavity provides enhanced performance by producing a completely new contact status with the ant's egg while caring for brood, relative to the uniaxial rotation existing in most other ant species. Despite the benefits to transporting ant eggs, the alteration of mandible postures resulting from biaxial rotation may introduce uncertainties to prey capture. However, our *in vivo* observations prove that the predation ability of ant *H. venator* remained effective while clutching prey of various sizes (**Fig. 3**). Using SEM technique, we find two, non-parallel rows of sharp teeth on its mandible inner surface (**Fig. 2B**), a special feature given many other ant species only have one row of teeth on each mandible (Gotwald, 1969). The morphological specialization is thus hypothesized to provide the ant with a means of compensating for the negative effects of the unusual biaxial rotation.

To put this hypothesis to the test, we quantitatively compare the tribological performance between five types of robotic mandibles (**Fig. 1C**) through the magnitudes of normal and friction forces and friction coefficient. According to comparison analysis, four interesting phenomena are discovered. First, comparing to mandibles with only one row of teeth, a remarkable augmentation in friction force is found in mandibles with two rows of teeth (**Fig. 5B**), potentially demonstrating the advantages of the feature that the ant has one more row of teeth on each mandible than most other ants. Second, dorsal teeth (DT) and ventral teeth (VT) have inverse variations in friction coefficient  $f$  resulting from the difference in their orientations (**Fig. 2B** and **Fig. 5C**). Moreover, the consistency of  $f$  between DT and DDT, as well as between VT and VVT, suggested that the key factor to change  $f$  is tooth orientation, rather than tooth number. Third, the friction coefficient  $f$  for DVT does not change as much as DDT and VVT with increasing rotation angle (**Fig. 5C**), according to their standard deviations (**Table 2**), and this can be well explained by the inverse variation in  $f$  between dorsal teeth and ventral teeth. In other words, the increase in  $f$  of DT compensates the decrease of VT, leading to the ignorable variations in  $f$  of DVT (**Fig. 5C**). Last, the ratio of compressive and shear moduli of the prey exoskeleton strongly influence the friction coefficient. When the ratio is lower than 0.5, mandibles may not be able to generate sufficient friction force to hunt prey with such a material property. In terms of prey's survival, it may have evolved exoskeleton that is much harder to penetrate than shear to resist against predators.

According to **Table 2**, the mean friction coefficient  $f$  of the ant mandibles with two non-parallel rows of teeth is 0.35. Since the friction force of the ant mandibles is previously reported as 192.24 mN (Zhang et al., 2020b) the corresponding normal force is estimated to be 549.26 mN, 1600 times the ant's weight (342.71  $\mu$ N). Considering the tremendous normal force, even a subtle variation in  $f$  would bring a great change in friction force and further influence the ant's tribological performance. The friction coefficient  $f$ , however, is closely related to the mandible postures that could be altered by the biaxial rotation, thereby depending on the featured dimension  $d$  of an object and the employed mandible region  $x$ . Considering the large range of the featured dimension and the elongated mandible, stabilizing  $f$  may be a great challenge for the ant. Through simulations of theoretical modelling under regimes of various  $d$  and  $x$ , significant variation in  $f$  occurs in all of the types of mandibles but DVT (**Fig. 6**). In other words, despite the randomness introduced by biaxial rotation, neither using different clamping regions nor processing prey of different sizes could change the friction coefficient for DVT mandibles much (**Fig. 6D**), demonstrating *H. venator*'s mandibles' excellent tribological stability resulting from specialized tooth design.

It is worth noting that the mandible of the trap-jaw ant *Acanthognathus* also has biaxial rotation and fang-like apical teeth consisting of three sharp teeth pointing in different directions (Gronenberg et al., 1998a). However, the functional relationship between the kinematic and morphological characteristics in the trap-jaw ant's mandibles remains a mystery. Similarly, the different orientations of teeth are probably an adaptive mechanism of biaxial rotation. This study can certainly provide an inspiration for comprehensively uncovering the mystery underlying the mandibles of *Acanthognathus*. In contrast to *Acanthognathus*, many other trap-jaw ants such as *Odontomachus* manipulate their mandibles uniaxially in a single plane. It would be interesting to investigate how *Acanthognathus* and *Odontomachus* employ their mandibles with different kinematics and morphology to achieve prey capture in a similar way, namely generating extreme striking force to stun prey. Even the mandibles of a single ant genus (*Strumigenys*) exhibit prominent morphological diversification associated with particular functions during evolution, which provides an ideal model for biomechanically investigating the relationship between morphology, kinematics and function (Booher et al., 2021). Moreover, various ant species use their mandibles to capture prey in diverse ways relying on the specialized microstructures and movements of mandibles (Dejean, 1985; Wesson and Wesson, 1939; Wilson, 1953; Masuko, 2009). For example, *H. venator* penetrates prey by double-rowed sharp teeth, whereas trap-jaw ants stun prey by striking at ultra-fast velocity with blunt teeth (Ehmer and Hölldobler, 1995). Therefore, future research can also focus on how the characteristics morphology and specialized kinematics renders the specialization of ant mandibles by conducting comparative biomechanical analysis involving different ant species of which mandibles have one or two rows of teeth and rotate biaxially or uniaxially. Addressing the biomechanics on the mandibles of ant individuals may shed lights on the diversity of ants' feeding habits and ecological niches (Brown Jr and Wilson, 1959).

Since ants are social insects, an ant colony usually has caste-based division of labor (Friedman

et al., 2019; Pennell et al., 2018). In *Myrmica* ants, queens are exclusively reproductive, major workers are responsible for power-demanding tasks such as defending and foraging, and minor workers engage in delicate tasks like nursing and brood care (Moffett, 1986; Molet et al., 2009; Molet et al., 2007). Due to the difference in the forces required by these tasks, the mandibles of major workers are more massive than those of minor workers (Larabee et al., 2018). However, such relationship between the tasks and mandible morphologies has not been found in the genus *Harpegnathos*. In *Harpegnathos*, not only queens, but also workers are reproductively totipotent (Gronenberg and Liebig, 1999; Liebig et al., 2000). Before workers become procreators (also known as gamergates), they have roles as foragers and hunt prey (Liebig et al., 1998). Therefore, the workers have to be able to engage in various tasks effectively (Zhang et al., 2020b). This study together with our previous research on adaptations for egg carrying (Zhang et al., 2020a) demonstrates that the sophisticated mandible morphology and the unique biaxial rotation kinematics together endows *H. venator* multifunctionality. We hypothesize that other ants with totipotent workers or otherwise reduced caste polymorphism should have similarly generalist mandibles, though the specific adaptations each species uses will likely vary (Farina et al., 2019).

To summarize, our theoretical modelling confirms that *H. venator*'s mandibles' specialized double-rowed teeth can produce a steady tribological performance under biaxial rotation pattern while clamping prey of various sizes. We also use physical models consisting of five different mandible-inspired paradigms for validation. These can also serve as a robotic prototype for next-generation, miniature grippers that can adaptively manipulate objects over a wide range of sizes with enhanced stability in tribological performance. Additionally, this study together with the previous ones revealed the multifunctional gripping mechanism underlying the ant mandibles (Zhang et al., 2020a). In detail, the combination of smooth concavities and biaxial rotation is responsible for handling objects like ant eggs gently, and the double-rowed, non-parallel teeth guarantee stable tribological performance for powerful clamping by eliminating the negative effects of biaxial rotation. The intrinsic connections among morphology, kinematics, and function in the ant mandibles shed lights on design of next-generation rigid, multifunctional robotic grippers.

## **Acknowledgement**

We thank Minghao Li and Zijin Guan from Sun Yat-Sen University for their assistance with filming predation behavior of the ant *Harpegnathos venator*. We would like to express our gratitude to EditSprings (<https://www.editsprings.com/>) for the expert linguistic services provided.

## **Competing interests**

The authors declare no competing or financial interests.

## **Funding**

This work was supported by the National Natural Science Foundation of China (grant no. 51905556), the Grant for Popularization of Scientific and Technological Innovation of Guangdong Province (grant no.2020A1414040007), and the research grant of Sun Yat-Sen University for Bairen

Plan (grant no.76200-18841223).

## Reference

- ALLEN, G. & CROFT, D. 1985. Soil particle size and the pit morphology of the Australian ant-lions *Myrmeleon diminutus* and *M. pictifrons* (Neuroptera: Myrmeleontidae). *Australian Journal of Zoology*, 33, 863-874.
- BHUSHAN, B. & NOSONOVSKY, M. 2004. Comprehensive model for scale effects in friction due to adhesion and two-and three-body deformation (plowing). *Acta materialia*, 52, 2461-2474.
- BOOHER, D. B., GIBSON, J. C., LIU, C., LONGINO, J. T., FISHER, B. L., JANDA, M., NARULA, N., TOULKERIDOU, E., MIKHEYEV, A. S. & SUAREZ, A. V. 2021. Functional innovation promotes diversification of form in the evolution of an ultrafast trap-jaw mechanism in ants. *PLoS biology*, 19, e3001031.
- BRITO, T. O., ELZUBAIR, A., ARAÚJO, L. S., CAMARGO, S. A. D. S., SOUZA, J. L. P. & ALMEIDA, L. H. 2017. Characterization of the mandible *Atta laevigata* and the bioinspiration for the development of a biomimetic surgical clamp. *Materials Research*, 20, 1525-1533.
- BROWN JR, W. L. & WILSON, E. O. 1959. The evolution of the dacetine ants. *The Quarterly Review of Biology*, 34, 278-294.
- BÜSSE, S., KOEHNSEN, A., RAJABI, H. & GORB, S. N. 2021. A controllable dual-catapult system inspired by the biomechanics of the dragonfly larvae's predatory strike. *Science Robotics*, 6.
- CERDÁ, X. & DEJEAN, A. Predation by ants on arthropods and other animals. 2011. National Academy of Sciences (US).
- DAS, S. & GHATAK, A. 2011. Puncturing of soft gels with multi-tip needles. *Journal of materials science*, 46, 2895-2904.
- DE FALCO, I., CIANCHETTI, M. & MENCIASSI, A. 2017. A soft multi-module manipulator with variable stiffness for minimally invasive surgery. *Bioinspiration & biomimetics*, 12, 056008.
- DEJEAN, A. 1985. An ecoethological study of predation in the ant genus *Smithistruma* (Formicidae: Myrmicinae, Dacetini). II. Attraction of the principal prey (Collembola). *Insectes sociaux= Social insects*.
- DONISTHORPE, H. 1937. A new species of *Harpegnathos* Jerd., with some remarks on the genus, and the other known species. (Hym. Formicidae). *Entomologists Monthly Magazine*, 73, 196-201.
- EHMER, B. & HÖLDOBLER, B. 1995. Foraging behavior of *Odontomachus bauri* on Barro Colorado island, Panama. *Psyche*, 102, 215-224.
- FARINA, S. C., KANE, E. & HERNANDEZ, L. P. 2019. Multifunctional structures and multistructural functions: integration in the evolution of biomechanical systems. *Integrative and comparative biology*, 59, 338-345.
- FRIEDMAN, N. R., REMEŠ, V. & ECONOMO, E. P. 2019. A morphological integration perspective on the evolution of dimorphism among sexes and social insect castes. *Integrative and comparative biology*, 59, 410-419.
- GHATAK, A. & DAS, A. L. 2007. Kink instability of a highly deformable elastic cylinder. *Physical review letters*, 99, 076101.
- GIULIETTI, F. & TORTORA, P. 2007. Optimal rotation angle about a nonnominal Euler axis. *Journal of guidance, control, and dynamics*, 30, 1561-1563.
- GOTWALD, W. H. 1969. *Comparative morphological studies of the ants, with particular reference to the mouthparts (Hymenoptera: Formicidae)*, Agricultural Experiment Station.
- GRONENBERG, W. 1996. The trap-jaw mechanism in the dacetine ants *Daceton armigerum* and *Strumigenys* sp. *Journal of Experimental Biology*, 199, 2021-2033.
- GRONENBERG, W., BRANDÃO, C. R. F., DIETZ, B. H. & JUST, S. 1998a. Trap-jaws revisited: the mandible mechanism of the ant *Acanthognathus*. *Physiological Entomology*, 23, 227-240.
- GRONENBERG, W., HÖLDOBLER, B. & ALPERT, G. D. 1998b. Jaws that snap: control of mandible movements in the ant *Myrmica*. *Journal of insect physiology*, 44, 241-253.
- GRONENBERG, W. & LIEBIG, J. 1999. Smaller brains and optic lobes in reproductive workers of the ant *Harpegnathos*. *Naturwissenschaften*, 86, 343-345.
- GRONENBERG, W., PAUL, J., JUST, S. & HÖLDOBLER, B. 1997. Mandible muscle fibers in ants: fast or powerful? *Cell and tissue research*, 289, 347-361.
- LARABEE, F. J., SMITH, A. A. & SUAREZ, A. V. 2018. Snap-jaw morphology is specialized for high-speed power amplification in the *Dracula* ant, *Myrmica camillae*. *Royal Society open science*, 5, 181447.
- LIEBIG, J., HÖLDOBLER, B. & PEETERS, C. 1998. Are ant workers capable of colony foundation? *Naturwissenschaften*, 85, 133-135.
- LIEBIG, J., PEETERS, C., OLDHAM, N. J., MARKSTÄDTER, C. & HÖLDOBLER, B. 2000. Are

- variations in cuticular hydrocarbons of queens and workers a reliable signal of fertility in the ant *Harpegnathos saltator*? *Proceedings of the National Academy of Sciences*, 97, 4124-4131.
- LIU, C., CHENG, J., LI, Z., CHENG, C., ZHANG, C., ZHANG, Y. & ZHONG, R. Y. 2020. Design of a self-adaptive gripper with rigid fingers for Industrial Internet. *Robotics and Computer-Integrated Manufacturing*, 65, 101976.
- MASUKO, K. 2009. Studies on the predatory biology of Oriental dacetine ants (Hymenoptera: Formicidae) II. Novel prey specialization in *Pyramica benten*. *Journal of Natural History*, 43, 825-841.
- MCINTOSH, S. H., AGRAWAL, S. K. & KHAN, Z. 2006. Design of a Mechanism for Biaxial Rotation of a Wing for a Hovering Vehicle. *IEEE/ASME Transactions on Mechatronics*, 11, 145-153.
- MOFFETT, M. W. 1986. Mandibles that snap: Notes on the ant *Myrmium camillae* Emery. *Biotropica*, 16, 361-362.
- MOLET, M., FISHER, B. L., ITO, F. & PEETERS, C. 2009. Shift from independent to dependent colony foundation and evolution of 'multi-purpose'ergatoid queens in *Myrmium* ants (subfamily Amblyoponinae). *Biological journal of the Linnean Society*, 98, 198-207.
- MOLET, M., PEETERS, C. & FISHER, B. L. 2007. Winged queens replaced by reproductives smaller than workers in *Myrmium* ants. *Naturwissenschaften*, 94, 280-287.
- PARK, H. & CHOI, H. 2012. Kinematic control of aerodynamic forces on an inclined flapping wing with asymmetric strokes. *Bioinspiration & biomimetics*, 7, 016008.
- PATEK, S., BAIQ, J., FISHER, B. & SUAREZ, A. 2006. Multifunctionality and mechanical origins: ballistic jaw propulsion in trap-jaw ants. *Proceedings of the National Academy of Sciences*, 103, 12787-12792.
- PENNEL, T. M., HOLMAN, L., MORROW, E. H. & FIELD, J. 2018. Building a new research framework for social evolution: intralocus caste antagonism. *Biological Reviews*, 93, 1251-1268.
- RESH, V. H. & CARDÉ, R. T. 2009. *Encyclopedia of insects*, Academic press.
- RICHTER, A., KELLER, R. A., ROSUMEK, F. B., ECONOMO, E. P., GARCIA, F. H. & BEUTEL, R. G. 2019. The cephalic anatomy of workers of the ant species *Wasmannia affinis* (Formicidae, Hymenoptera, Insecta) and its evolutionary implications. *Arthropod structure & development*, 49, 26-49.
- SPAGNA, J. C., SCHELKOPF, A., CARRILLO, T. & SUAREZ, A. V. 2009. Evidence of behavioral co-option from context-dependent variation in mandible use in trap-jaw ants (*Odontomachus* spp.). *Naturwissenschaften*, 96, 243-250.
- SUI, D., ZHU, Y., ZHAO, S., WANG, T., AGRAWAL, S. K., ZHANG, H. & ZHAO, J. 2020. A Bioinspired Soft Swallowing Gripper for Universal Adaptable Grasping. *Soft Robotics*.
- URBANI, C. B., BOYAN, G. S., BLARER, A., BILLEN, J. & ALI, T. M. 1994. A novel mechanism for jumping in the Indian ant *Harpegnathos saltator* (Jerdon)(Formicidae, Ponerinae). *Experientia*, 50, 63-71.
- WESELOH, R. M. & HARE, J. D. 2009. Predation/predatory insects. *Encyclopedia of insects*. Elsevier.
- WESSON, L. G. & WESSON, R. G. 1939. Notes on *Strumigenys* from southern Ohio, with descriptions of six new species. *Psyche*, 46, 91-112.
- WILSON, E. O. 1953. The ecology of some North American dacetine ants. *Annals of the Entomological Society of America*, 46, 479-495.
- ZHANG, W., HE, Z., SUN, Y., WU, J. & WU, Z. 2020a. A Mathematical Modeling Method Elucidating the Integrated Gripping Performance of Ant Mandibles and Bio-inspired Grippers. *Journal of Bionic Engineering*, 17, 732-746.
- ZHANG, W., LI, M., ZHENG, G., GUAN, Z., WU, J. & WU, Z. 2020b. Multifunctional mandibles of ants: Variation in gripping behavior facilitated by specific microstructures and kinematics. *Journal of insect physiology*, 120, 103993.